



Deposited via The University of Sheffield.

White Rose Research Online URL for this paper:

<https://eprints.whiterose.ac.uk/id/eprint/129649/>

Version: Accepted Version

Article:

Russell, J., Owen, J. and Hajirasouliha, I. (2018) Nonlinear behaviour of reinforced concrete flat slabs after a column loss event. *Advances in Structural Engineering*, 21 (14). pp. 2169-2183. ISSN: 1369-4332

<https://doi.org/10.1177/1369433218768968>

Russell JM, Owen JS, Hajirasouliha I. Nonlinear behaviour of reinforced concrete flat slabs after a column loss event. *Advances in Structural Engineering*. 2018;21(14):2169-2183. Copyright © 2018 The Author(s). DOI: <https://doi.org/10.1177/1369433218768968>. Article available under the terms of the CC-BY-NC-ND licence (<https://creativecommons.org/licenses/by-nc-nd/4.0/>).

Reuse

This article is distributed under the terms of the Creative Commons Attribution-NonCommercial-NoDerivs (CC BY-NC-ND) licence. This licence only allows you to download this work and share it with others as long as you credit the authors, but you can't change the article in any way or use it commercially. More information and the full terms of the licence here: <https://creativecommons.org/licenses/>

Takedown

If you consider content in White Rose Research Online to be in breach of UK law, please notify us by emailing eprints@whiterose.ac.uk including the URL of the record and the reason for the withdrawal request.

1

Nonlinear behaviour of reinforced concrete flat slabs after a column loss event

Journal Title

XX(X):2–30

©The Author(s) 2018

Reprints and permission:

sagepub.co.uk/journalsPermissions.nav

DOI: 10.1177/ToBeAssigned

www.sagepub.com/



2 **J.M. Russell¹, J.S. Owen² and I. Hajirasouliha³**

Abstract

Previous studies have demonstrated that reinforced concrete flat slab structures could be vulnerable to progressive collapse. Although such events are highly dynamic, simplified static analyses using the sudden column loss scenario are often used to gain an indication into the robustness of the structure. In this study, finite element analysis is used to replicate column loss scenarios on a range of RC flat slab floor models. The model was firstly validated against the results of scaled slab experiments and then used to investigate the influence of different geometric and material variables, within standard design ranges, on the response of the structure. The results demonstrate that slab elements are able to effectively redistribute loading after a column loss event, and therefore prevent a progressive collapse. However, the shear forces to remaining columns were 159% of their fully supported condition and increased to 300% when a dynamic amplification factor of 2.0 was applied. It is shown that this can potentially lead to a punching shear failure in some of the slab elements.

Keywords

4 Progressive Collapse, Column Loss, RC Flat Slab, Punching Shear

5 Introduction

6 Since the collapse of Ronan Point tower building in 1968 the issue of progressive
7 collapse of structures has been an important consideration for structural engineers. Much
8 research has been aimed at understanding the response of different structural systems
9 to a damaging event, commonly using the sudden column loss scenario. Extensive
10 studies have covered the experimental, theoretical and numerical analysis of steel and
11 Reinforced Concrete (RC) frame structures (Sasani et al. 2007; Flint et al. 2007; Yi
12 et al. 2008; Su et al. 2009; Valipour and Foster 2010; Qian and Li 2013; Pham and
13 Tan 2017). However the nature of flat slab construction creates a different response
14 to extreme events compared to beam structures as a slab is able to redistribute forces
15 more effectively. Previous events have demonstrated that flat slabs can be susceptible to
16 progressive collapse, as seen with the Piper's Row car park, UK, in 1998 (Whittle 2013)
17 or Sampoong department store, South Korea, 1995 (Gardner et al. 2002; Park 2012). RC
18 Slabs can undergo brittle failure due to punching shear or exhibit geometric nonlinearity
19 in the form of tensile or compressive membranes (Hawkins and Mitchell 1979; Mitchell
20 and Cook 1984; Muttoni 2008; Qian and Li 2012; Dat and Hai 2013; Keyvani et al.
21 2014).

22 Finite Element (FE) analysis has been used successfully to model the response of
23 structures to extreme events such as column loss, typically for framed structures (Kokot
24 et al. 2012; Fu 2010; Kwasniewski 2010) and has been shown to suitably consider
25 the nonlinear aspects involved. FE analysis has also been successfully used for RC
26 slab sections (Trivedi and Singh 2013; Li and Hao 2013), including consideration of
27 shear capacity (Mamede et al. 2013). However, accurate modelling of the post-punching
28 behaviour remains a challenge for FE packages despite the work of others (Faria et al.
29 2012; Ruiz et al. 2013; Mirzaei and Sasani 2013; Genikomsou and Polak 2015).

¹School of Engineering, University of Warwick, Coventry, UK

²Faculty of Engineering, The University of Nottingham, UK

³Department of Civil and Structural Engineering, The University of Sheffield, UK

Corresponding author:

Justin Russell, School of Engineering, University of Warwick, Coventry, UK

Email: j.russell.3@warwick.ac.uk

30 Furthermore, after Liu et al. (2015)'s important work into the response of flat slab
31 structures to progressive collapse highlights that such structures can be highly susceptible
32 to extreme events and that further studies are needed. As the potential for progressive
33 collapse is dependant on the whole structural response it is important to consider the
34 behaviour of a full floor section to consider the complete performance and what factors
35 influence it. In particular the extent of damage and the potential for punching shear failure
36 should be addressed.

37 This study therefore investigated the effect of column loss on a large RC flat slab
38 floor structure. The main objectives are to demonstrate how the loading is redistributed,
39 determine the extent of damage this causes, identify the potential overloading of
40 surrounding columns and consider how geometric and material variations affect this.
41 An FE model of a flat slab structure was validated against a series of experimental tests
42 on scaled substructures and then a static push down analysis was conducted focusing on
43 the nonlinear behaviour and the redistribution of forces after a column loss. The Critical
44 Shear Crack Theory (CSCT) was applied to the surrounding columns to determine which
45 areas and conditions might be susceptible to punching shear and would therefore require
46 more detailed consideration.

47 **Description of FE model**

48 To assess the response of a concrete flat slab structure to column loss event, a FE model
49 was created and analysed using Abaqus/Explicit (Simulia 2010). Solid, 8 node, brick
50 elements (C3N8R) with reduced integration were used to model the concrete sections.
51 Geometric non-linearities, for example compressive membrane action, are also taken into
52 account by using such an approach. The nonlinear behaviour of the concrete was defined
53 using the Concrete Damaged Plasticity (CDP) model suggested by Lubliner et al. (1989)
54 and modified by Lee and Fenves (1998) which is based on a Drucker-Prager hyperbolic
55 function. This damage model considers the behaviour of the concrete after cracking
56 as a region of plastic strain, in effect representing a continuum of micro-cracks. This
57 model has been regularly used for considering damage to concrete sections (Cicekli et al.
58 2007; Genikomsou and Polak 2015) due to its general purpose application for static and
59 dynamic modelling of concrete. Full details can be found in the Abaqus manual (Simulia
60 2010). The uniaxial stress-strain behaviour of concrete in compression, after the linear
61 elastic phase, is modelled with Equation 1 from CEB-fib du Béton (2012):

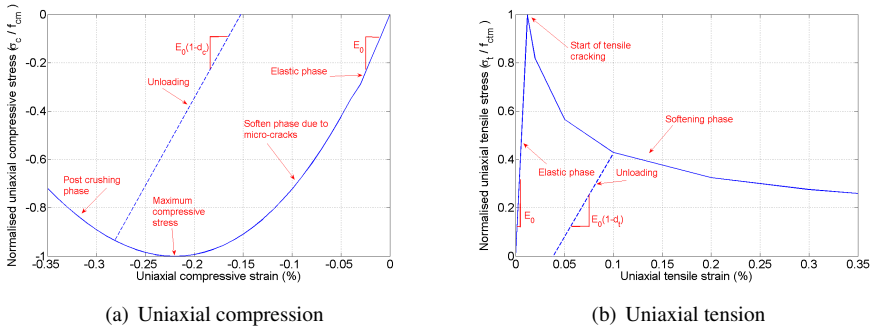


Figure 1. Annotated concrete stress-strain models

$$\sigma_c = -f_{cm} \left(\frac{k \cdot \eta - \eta^2}{1 + (k - 2) \cdot \eta} \right) \quad (1)$$

62 where $\eta = \epsilon_c / \epsilon_{c1}$, i.e. the ratio of compression strain to crushing strain, and k is the
 63 plasticity number taken as 2.15 for C25/30 concrete. This gives a parabola shape beyond
 64 the elastic limit (see Figure 1(a)), with a softening effect until the ultimate limit, f_{cm} ,
 65 due to compressive micro-cracks. After this point, there is a reduction in capacity as the
 66 concrete crushes. However, from all the scenarios considered with this FE model, only in
 67 the most extreme cases was the compression ultimate limit exceeded and so the material
 68 definition for this range is not believed to be critical to the results.

69 In tension, concrete is taken to be linear elastic up to its cracking stress, after which a
 70 nonlinear tension softening model is used to account for the reduction in the capacity of
 71 concrete. This is described Figure 1(b) according to Okamura and Maekawa (1990).

$$\sigma_t = \begin{cases} E_0 \cdot \epsilon_t & \text{for } \sigma_t \leq f_{ctm} \\ f_{ctm} \cdot \left(\frac{\epsilon_t \cdot ck}{\epsilon_t} \right)^{0.4} & \text{for } \sigma_t > f_{ctm} \end{cases} \quad (2)$$

72 Additionally, account is made for the permanent reduction in elastic stiffness after
 73 crushing or cracking by use of a damage index, d_t or d_c for tension and compression
 74 respectively. These parameters are considered to be proportional to the maximum stress
 75 in each direction and vary from 0 for before the ultimate tensile or compressive stress is
 76 reached, up to 1 for a complete loss of stiffness (Simulia 2010).

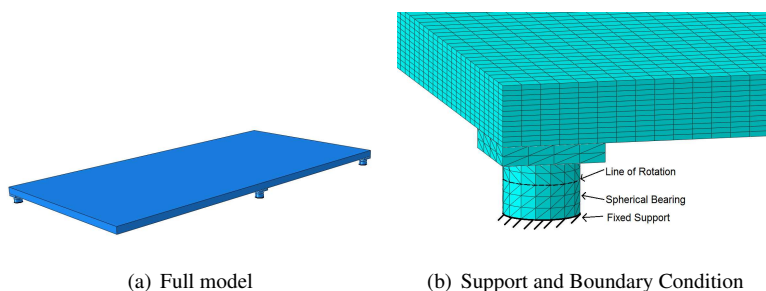
77 For the concrete plastic model it requires the following inputs, the Dilation angle (ψ)
78 was taken as 35° , an eccentricity (m) of 0.1, K_c factor of 2/3, ratio of initial equibiaxial
79 compressive yield stress to initial uniaxial compressive yield stress (σ_{b0}/σ_{c0}) of 1.16 and
80 a viscosity parameter of 0. These definitions and the values used come from the Abaqus
81 user manual (Simulia 2010) and are all default values which convert the uniaxial stress
82 strain relationship for compression and tension into the yield surface (Jankowiak and
83 Lodygowski 2005).

84 The steel reinforcement was modelled with circular beam elements, element ID
85 B31. The bond between the steel bars and the concrete was achieved by using
86 Abaqus's embedded region feature, which constrains the translational degree between
87 the elements nodes (Simulia 2010). Additionally, full bond was assumed between the
88 steel and concrete, including along the entire anchorage length. Although this potentially
89 overestimates the capacity provided by the steel in these regions, since no bar pull out
90 was observed during the experimental validation tests, this simplification is considered
91 adequate. Furthermore, as the Critical Shear Crack Theory, rather than FE results, was
92 used for estimating shear strength, this approach is suitable for considering the response
93 up to punching shear failure.

94 Solutions from nonlinear FE analysis are usually influenced by the mesh refinement.
95 While a coarse mesh will not replicate the true stress gradients across a section, if there
96 are localised areas of high tensile stress, decreasing the mesh size results in narrower
97 crack bands and may not represent true distribution of stresses and strains. To determine
98 a suitable mesh density, a mesh sensitivity study was conducted on the model for the
99 corner removal with static loading condition (test C-S). It was found that using concrete
100 elements 25mm wide by 6.67mm deep and 100mm rebar elements, which resulted
101 in a model with 165312 elements requiring 264 hours of computational time, was a
102 suitable balance between computational time and accuracy. In general, this refinement
103 overestimates the deflections at the highest loading levels but it shows a good agreement
104 within the elastic range and into the early cracking phase. For example, Table 1 compares
105 the results of the mesh sensitivity analyses for the corner removal (test C-S). More
106 information on about the mesh refinement can be found in Russell (2015). Figure 2 shows
107 the meshed FE model. The bearing supports, as used in the experimental programme, can
108 also be seen. These are fixed at their base but allow separation and rotation between the
109 steel components.

Table 1. Results from mesh sensitivity study

	Coarse	Fine	Very Fine	Experimental	
No. of concrete elements	27552	165312	344400		
Slab Element Width (mm)	50	25	20	N/A	
Slab Element Depth (mm)	10	6.67	5		
Rebar Element Length (mm)	200	100	50		
Peak displacement at: (mm)	3.0kN/m ²	4.40	4.57	4.52	4.8
	6.0kN/m ²	15.00	18.44	18.01	15.1
	7.5kN/m ²	44.95	67.91	87.24	63.8
Computational Time (Hr)	28	264	431	N/A	

**Figure 2.** Rendering of the FE model showing mesh and boundary conditions

Validation against experimental results

110

111 Two static loading tests of RC flat slab substructures conducted by Russell et al. (2015)
 112 were replicated to validate the FE models. Both tests were based on a 2x1 bay 1/3 scale
 113 slab substructures as shown in Figure 3. Two column removal scenarios with uniformly
 114 distributed loads (UDLs) were considered, the loss of a corner (C) column and the
 115 loss of an edge column causing a penultimate (P) column loss (i.e. the bottom left and
 116 bottom middle columns in Figure 3 respectively). An FE model based on the geometry
 117 of the experimental slabs was constructed. Concrete and steel properties required for
 118 the material models were determined from tests conducted on samples taken during the
 119 experimental programme.

120 Support reactions were measured during the testing with load cells so comparisons
 121 could be made with the calculated values from the FE. The displacement readings
 122 recorded from LVDTs, were compared against nodal displacements at the equivalent
 123 positions. The locations of monitored points for displacements are shown in Figure 3.

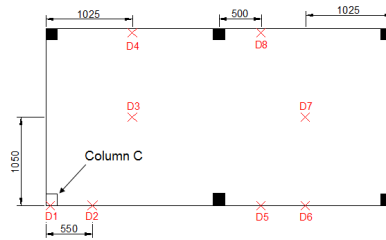


Figure 3. Locations of LVDTs and visual targets (D) from experiential programme for corner removal condition (Russell et al. 2015)

124 The final crack locations from the experiment were also compared to the plastic strain
 125 distributions in the concrete slab elements.

126 *Force redistribution*

127 The relative load on each support after a corner column removal case (test C-S) is
 128 shown in Figure 4. The solid lines show the FE results while the data points from the
 129 experimental test are also plotted to allow comparison. For all positions and for most of
 130 the loading, a very similar response is observed. There is a higher deviation at higher
 131 load levels (i.e. $UDL > 6\text{kN/m}^2$), with a maximum difference of 3.6 percentage points.
 132 This is due to the effects of cracking in the concrete, which reduces the stiffness around
 133 the supports. It should be mentioned that the proposed model does not capture this effect
 134 fully, partly because the plastic damage rule used leads to a gradual reduction in stiffness
 135 after cracking, whilst concrete often undergoes a sudden change. However, past the initial
 136 cracking phase there is again a strong agreement between the results and the overall
 137 response is considered to be good enough to make predictions on the demand placed on
 138 surrounding supports after a column loss.

139 *Displacements*

140 The force-displacement diagram is one of the key indicators into the suitability of the
 141 FE model as it allows validation of the elastic response of a structure and identifies the
 142 onset of cracking. It can also provide an indication of the ductility of the structure in
 143 the nonlinear range. As expected, at all recorded points there is an initial linear force-
 144 displacement response, however, once cracking starts to occur, there is a significant
 145 reduction in stiffness. Considering the displacement against loading for the corner

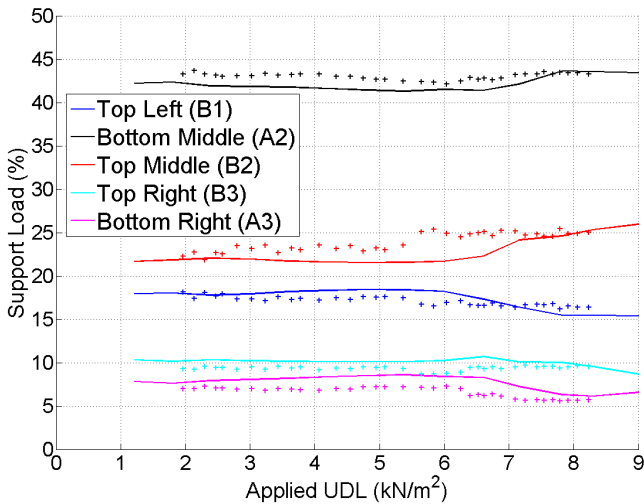


Figure 4. Distribution of forces to each support as loading increases. Test C-S. Solid line is FE model, +'s the experimental results

146 column loss condition shown in Figure 5, there is a very good agreement between the
 147 FE model and the experimental results. The locations of the monitored points were given
 148 in Figure 3. Both the positions presented match the initial stiffness of the experimental
 149 results at low levels of loading. After cracking occurs there was a sudden increase in
 150 displacements observed in the experimental case, however the FE model gives a more
 151 gradual response. This matches the tensile response of concrete described by Equation 2.
 152 Despite this effect, variation between the cases remains small for the whole range of load
 153 applied.

154 *Flexural damage*

155 It is important to consider the location and extent of damage when assessing the effect of
 156 a column loss on a structure. The finite element analysis gives an indication of the areas
 157 that might experience damage or cracking and these were compared with the cracking
 158 patterns from the experimental results.

159 The CDP model considers cracks to be a region of plastic deformation. Therefore, the
 160 location of the plastic strains should correspond to the location of cracks observed from
 161 the experimental case; this is compared in Figure 6. The location of cracks and plastic

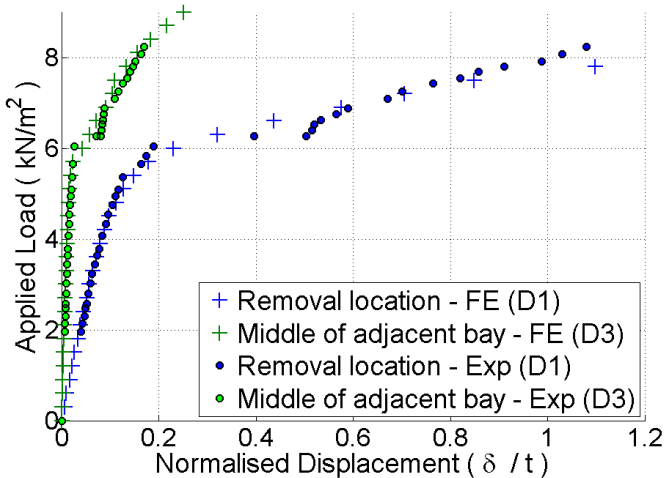


Figure 5. Normalised displacement against load for test comparing experimental results to the FE. Test C-S

162 strains (Figures 6(a) and 6(b) respectively) after a corner column loss, with 7.8kN/m^2 of
 163 loading is shown. The cracks and plastic strain follow the sagging yield lines acting
 164 between the supports and the damage occurs across most of the slab, with the most
 165 extensive effects close to the remaining corner support. In the adjacent bay the cracks can
 166 be seen to follow the reinforcement locations, which are also annotated, as was seen from
 167 the experimental results. On the top surface the cracks/plastic strains run between the
 168 supports with most of the damage concentrated in a fanning pattern of cracks around the
 169 middle supports (contrasting the radial pattern seen on the underside), which identifies
 170 the hogging yield lines resulting from the non-regular layout of remaining supports.
 171 All these patterns fit closely with the observed results discussed in more detail in the
 172 experimental work (Russell et al. 2015).

173 In general, the presented FE model correlates well to the results from the experimental
 174 slabs. In particular, the changes in reaction forces after a column loss show a close
 175 similarity, as do the locations of concrete cracks. This indicates that the stress distribution
 176 of FE model matches the true non-linear behaviour after a column loss scenario. The
 177 static displacements against load also correspond well between the experimental and FE
 178 cases, especially at the low loading levels. The higher loading conditions showed higher
 179 deviations due to the difficulty in defining the material properties for reinforced concrete

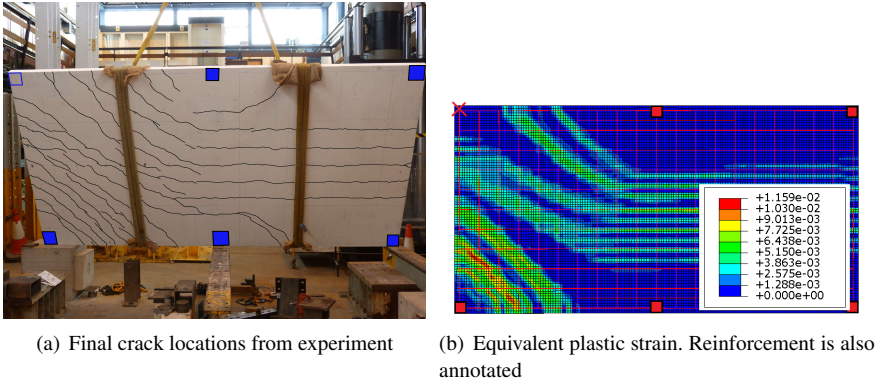


Figure 6. Comparisons of bottom surface cracking patterns at 7.8kN/m^2 of loading for test C-S

Table 2. Values for the dimensions in Figure 7 used for the parameter study

Symbol	Label	Values (mm)
L	Span length	4000, 5000 and 6000
t	Slab thickness	180, 200, 250 and 300
L_{over}	Overhang	200
c	Column width	400
H	Storey height	3000

180 after extensive cracking has occurred for two-dimensional elements such as slabs. This
 181 leads to uncertainty in modelling the required nonlinear relationships for the extreme
 182 range. However, this occurs at higher deformations than is typical for accidental loading
 183 cases and so the proposed approach is considered suitable for the the range of conditions
 184 expected. Further information about the reference experimental tests and validation of
 185 the FE models can be found in Russell (2015).

186 Description of floor model

187 The validated FE model was extended to investigate the influence of changing different
 188 design parameters on the response of typical structures after a column loss event. A
 189 plan and elevation of the floor model is shown in Figure 7. Table 2 lists the geometric
 190 dimensions that were varied for the parameter study. The values used were limited by
 191 common configurations and the requirement to meet design guidelines.

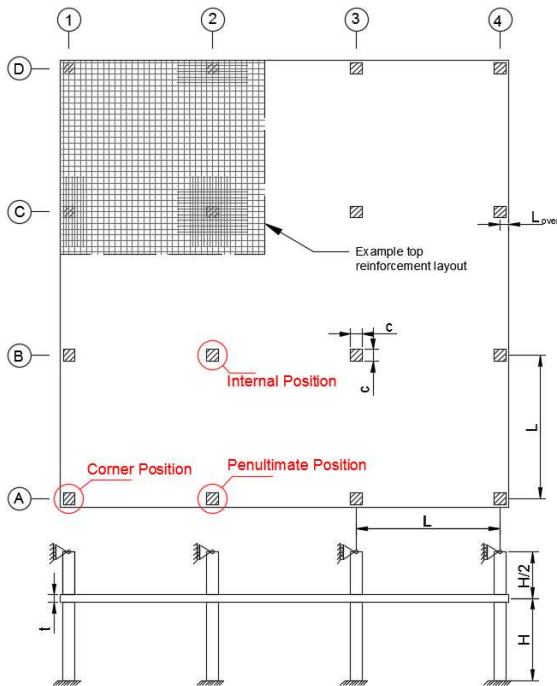


Figure 7. Plan and elevation showing labels, key column locations, typical reinforcement and grid markings

192 Each of the models was designed to meet current Eurocode requirements according
 193 to EN 1992 (2004). The structures were analysed using the equivalent frame method to
 194 obtain the required bending moments and shear forces. Characteristic dead loading was
 195 based on the selfweight of the material, taken as 25kN/m^3 , plus an additional 1.0kN/m^2
 196 to account for other finishes. Live loading for design was taken at 2.5kN/m^2 . Unless
 197 otherwise stated, the characteristic compressive concrete strength was 30MPa . Based
 198 on the design forces, adequate flexural steel was provided, including the requirement
 199 to place 50% of the tensile steel for hogging moments within 0.125 times the span
 200 width. To meet durability specifications, 25mm of cover was provided to all steel. In
 201 all locations, for both top and bottom steel, at least a minimum area of steel was provided
 202 according to Eurocode requirements. Each model configuration met the required shear
 203 stress capacity without the inclusion of extra reinforcement. As the size of the columns
 204 was kept constant, the maximum span to depth ratio considered was limited by the shear
 205 capacity of the concrete.

Table 3. Span length and slab thickness for each model

Span length L (mm)	Slab thickness t (mm)	Effective span L_{eff}	Span to depth ratio L_{eff}/t
4000	180	3780	21.0
4000	200	3800	19.0
4000	250	3850	15.4
5000	200	4800	24.0
5000	250	4850	19.4
5000	300	4900	16.3
6000	250	5850	23.4

206 In total, seven different arrangements were considered as listed in Table 3. The span
207 to depth ratios are based on the effective span length, L_{eff} , of an internal bay with a
208 continuous slab over the supports according to Equation 3. These represent the range of
209 span to depth ratios that are typical for flat slabs without shear reinforcement, i.e. 15–25.

$$L_{eff} = L - 2\left(\frac{c}{2}\right) + 2\left(\frac{t}{2}\right) \quad (3)$$

210 where the terms L , c and t are the span length, column width and slab thickness
211 respectively, as identified in Figure 7 and Table 2. All bays were square and had the
212 same span lengths, i.e. the aspect ratio of both the bays and the entire floor was constant.

213 *Loading on the slab*

214 For the FE simulations a UDL was applied to the entire slab area and was linearly
215 increased up to the accidental load combination, w_{ac} , as given in Equation 4 from US
216 General Services Administration (GSA) (2013), where DL and LL are the Dead and Live
217 Loads respectively. While other load factors could be used to account for loading during
218 an accidental event, this requirement is one of the highest commonly used.

$$w_{ac} = 1.2DL + 0.5LL \quad (4)$$

219 Once this level was reached, a further UDL was applied only to the bays around the
220 lost column. The loading in this area was increased linearly up to a value of $2w_{ac}$, i.e. a
221 Dynamic Amplification Factor (DAF) of 2.0. This additional load replicates the dynamic
222 influence affecting those bays (Tsai and Lin 2009).

223 *Punching shear calculations*

224 Modelling of punching shear failure in finite element software is possible but requires
 225 the connections to be very carefully defined and the failure is more sensitive to mesh
 226 arrangement and the modelling solver. As has been demonstrated by others such as
 227 Genikomsou and Polak (2015), consideration of punching shear failure for a single
 228 connection is a demanding problem. For the size of floor slabs considered in this study, it
 229 would not be efficient to model the connections for this. Additionally, this work is focused
 230 on the response of the slab before punching shear failure and the potential complete
 231 collapse this could cause. As such, crack patterns, force redistributions, the displacement
 232 response and their relation to different column removal cases and geometric and material
 233 variables are not dependant on the shear approach used. Therefore each simulation was
 234 run to full loading and excluded shear failure and the punching shear capacity of the
 235 unreinforced flat slab connections was estimated with the Critical Shear Crack Theory
 236 (CSCT) developed by Muttoni (Muttoni 2008). The CSCT has been demonstrated to be
 237 suitable for assessing progressive collapse of flat slab structures (Micallef et al. 2014;
 238 Liu et al. 2015; Olmati et al. 2017) and the equation for predicting shear strength without
 239 transverse reinforcement is given in Equation 5, shown below,

$$\frac{V_R}{b_o d \sqrt{f_{ck}}} = \frac{3/4}{1 + 15 \frac{\psi d}{d_{go} + d_g}} \quad (5)$$

240 where V_r is the shear force strength of the connection, b_o is the shear perimeter including
 241 a reduction to account of eccentric loading, d is the slab depth, f_{ck} is the concrete
 242 compressive strength, d_g is the aggregate diameter, ψ is the rotation of the slab, and
 243 is used as a proxy for crack width. The rotations and reactions were taken from the
 244 nonlinear finite element model which corresponds to a Level IV approximation from the
 245 Model Code 2010 (2012).

246 **FE analysis results and discussion**

247 *Concrete cracking*

248 During the analysis, cracking in the concrete elements was monitored to understand
 249 which areas of the structure were susceptible to flexural damage. The following results
 250 are based on the response of the model with a span to depth ratio of 19.4. However, it
 251 was seen that increasing the span to depth ratio primarily causes nonlinear behaviour due
 252 to cracking to occur earlier, but does not change the stress distribution and progression of

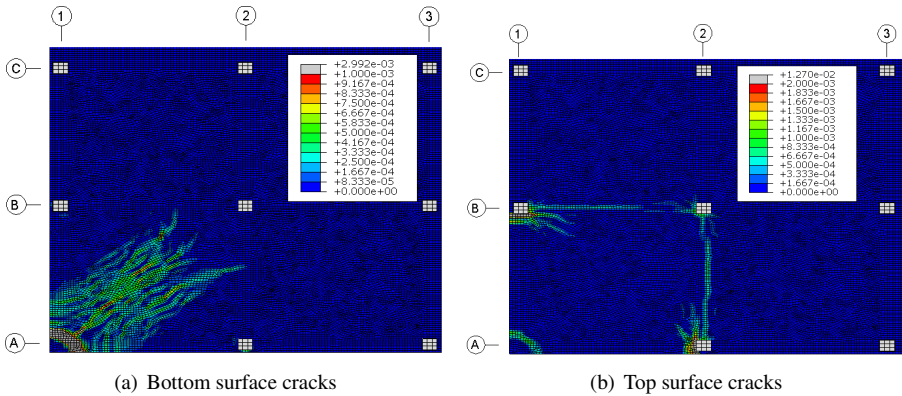


Figure 8. Location of tensile plastic strain regions in the concrete elements after corner column (A1) removal; $w = 2w_{ac}$

253 damage patterns. Figure 8 shows the location and extent of plastic strains, representing
 254 cracks, that occurred after a corner column loss. Minimal plastic damage was observed
 255 before $1.5w_{ac}$. On the bottom surface (Figure 8(a)) diagonal cracks develop between the
 256 two orthogonally adjacent supports, as was observed during the experimental programme
 257 (Russell et al. 2015). However, these are limited to the bay directly around the removed
 258 column. On the top surface (Figure 8(b)) the cracks span between the surrounding
 259 supports, although the locations directly adjacent to the columns remain the most critical
 260 areas. Additionally, the start of a diagonal crack between columns A2 and B1 can be
 261 seen.

262 After an internal column removal, a similar response is observed with cracks
 263 concentrated directly next to the adjacent supports at relatively low loading (see Figure
 264 9). By increasing the load, a large area of the structure is affected by extensive cracking
 265 on both the bottom surface (Figure 9(a)) and the top surface (Figure 9(b)). These plastic
 266 strains are larger, and cover more of the structure, than the corner condition, which
 267 explains why the internal column removal case has higher displacements, as shown later.
 268 It can also be noted that the hogging moments create cracks that surround the damaged
 269 bay and the sagging condition results in many cracks in the middle of the bay, however,
 270 the rest of the structure remains largely unaffected.

271 These cracking patterns demonstrate the change in stress distribution for a structure
 272 that has lost a column. For sagging moments, it is clear there is significant stress acting
 273 between diagonal columns (see B1-A2 for both presented cases). On the top surface the

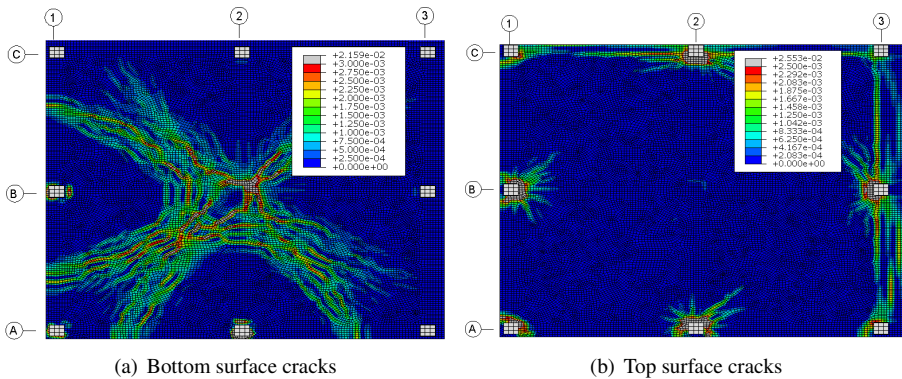


Figure 9. Location of equivalent plastic strain regions in the concrete elements after internal column (B2) removal; $w = 2w_{ac}$

274 stress distribution has changed from the pattern expected for a regular column layout
 275 and now act perpendicular to grid line C1-C2 for internal case as well as towards the
 276 removed column location, perpendicular to line A2-B3, B3-C2 etc. The pattern of cracks
 277 match these seen in the experimental programme and the FE validation for the small
 278 slab section. In particular the radial yield lines around the remaining supports on the
 279 underside can be seen while on the top surface there is a fanning pattern around the
 280 adjacent supports after a column removal. Additionally, there is a clear hogging yield
 281 line acting between supports.

282 These concrete cracking patterns highlight the important changes to the internal forces
 283 in the slabs as a column loss event. For a flat slab with a regular arrangement of columns
 284 there is the traditional bending moment response along the grid lines. However, after a
 285 column removal event the span length will not be doubled, as would be predicted for
 286 a beam system, and a new bending moment arrangement forms utilising the shorter
 287 diagonal distance. Therefore the area around the removed column, although originally
 288 designed as a hogging moment location, may experience some sagging (particularly in
 289 an internal column removal case). The area of largest sagging bending stress is likely to
 290 be around the middle of the bay, which was designed for a sagging condition. However,
 291 the hogging bending stresses clearly extend to areas which were not intended for such
 292 conditions and may exceed their tensile capacity.

293 Understanding these effects is important for considering efficient changes to design
 294 for reducing damage after a column loss events.

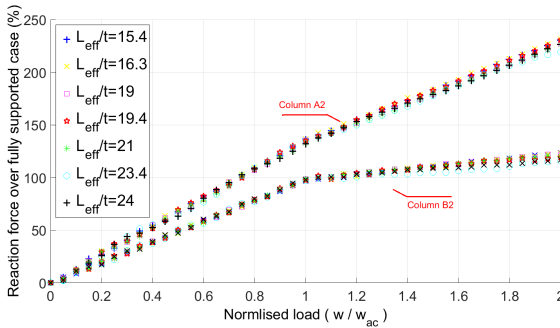


Figure 10. Change in column reaction forces due to static load increases for different span to depth ratios. Corner column removal

Reaction forces

295

296

297

298

299

300

301

302

303

304

305

306

307

308

309

310

311

312

313

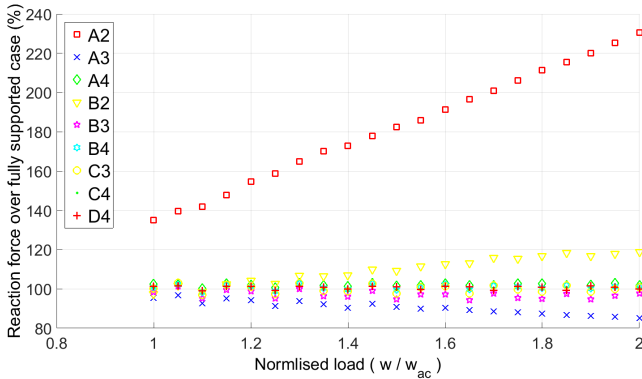
314

315

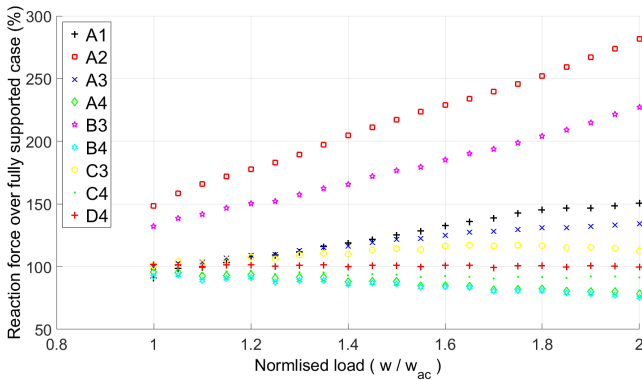
316

Figure 10 shows the sum of reaction forces at two column bases as the static load is increased after a corner column loss. Column A2 is an orthogonally adjacent column to the removed location, see Figure 7, and experiences the highest increase in reaction force. For further comparison, column B2 is shown. The experimental programme indicated that this location (i.e. across the diagonal from the removed column) experienced a reduction in its relative loading (reaction force over fully supported case) as a result of the column loss. The seven models with different span to depth ratios are plotted and the reaction forces normalised against the fully supported condition with a load of w_{ac} . The main observation is that there is no significant difference in relative demand for structures with different span to depth ratios. As a result, all other comparisons will be made with just one configuration, $L_{eff}/t=19.4$. At a loading of $w = w_{ac}$ applied to the entire structure, column B2 exhibits a relative load of slightly less than 100%, demonstrating the demand is reduced. However, increasing the load in the critical bay results in a slight increase in loading at this location.

After a column loss, some of the remaining columns can experience a significantly higher load than they were previously carrying. This can be seen further in Figure 11, which shows the change in the column load, compared to its fully supported condition, for all the remaining columns after a corner (Figure 11(a)) or internal (Figure 11(b)) column loss. Due to the symmetry of the structure only half the columns are plotted. It can be seen from the results that the two orthogonally adjacent columns have the largest increase in vertical loading. As was observed during the experimental programme, there



(a) Corner column removal (A1)



(b) Internal column removal (B2)

Figure 11. Change in column reaction forces due to static load increases. $L_{eff}/t=19.4$

317 is a linear increase in the loads transferred to each support, as total load is increased.
 318 However, it can be seen that at the higher loadings the effect of damage around the
 319 column changes this response as the slab is no longer truly continuous over the support
 320 and so force distributions change.

321 The highest relative increase in loading to a column for each scenario is given in Table
 322 4. It is shown that, even without additional loading to account for dynamic effects, these
 323 locations were overloaded by at least 35%. As the load factor was increased to 2.0, critical
 324 columns are overloaded by up to 3 times their fully supported condition. Furthermore,
 325 although removing two columns could appear to be more critical scenario, as such an

Table 4. Summary of static reaction forces at remaining columns

Removed column(s)	Critical column(s)	Increase in reaction at:	
		w_{ac}	$2w_{ac}$
Corner (A1)	A2/B1	135%	231%
Internal (B2)	A2/B1	148%	282%
Penultimate (A2)	A1	158%	301%
Two Column (A1 and A2)	A3	159%	251%

event influences a larger portion of the structure, the load can be redistributed to more columns and reduces the demand on a single location. This is seen in Table 4 where by the final loading, there is a larger maximum increase for Internal or Penultimate column removals than when two edge columns are removed.

Displacement response

In this study, to compare the effects of using different geometries, a displacement ductility factor μ_δ , is used as given in Equation 6

$$\mu_\delta = \frac{\delta}{\delta_y} \quad (6)$$

where δ and δ_y are the displacement and the yield displacement of the removal point respectively. The yield displacement is obtained for each analysis by fitting a bilinear relationship to the response with the requirement to ensure the area under the simplified model is equal to the area under the measured curve. As δ/t (t =slab thickness) is also a common relationship in considering the relative magnitude of the deflections on the structure, both this ratio and the ductility factor will be used to discuss the response.

Figure 12 shows the corner displacement results for each span to depth ratio, normalised against the yield displacement. It is shown that there is a relationship between increasing the span to depth ratio and the ductility indicating more flexible slabs will exhibit more material nonlinearity within the loading range considered for design. Additionally, for configurations with a smaller L_{eff}/t , compressive membrane action can increase the stiffness of the slab reducing the damage and displacements Keyvani et al. (2014).

The displacement results of the corner removal case are presented in Table 5. The yield displacement varies between 0.013 and 0.067 times the slab depth. Up to the accidental load case, there are small displacements for all cases and usually a good linear trend is

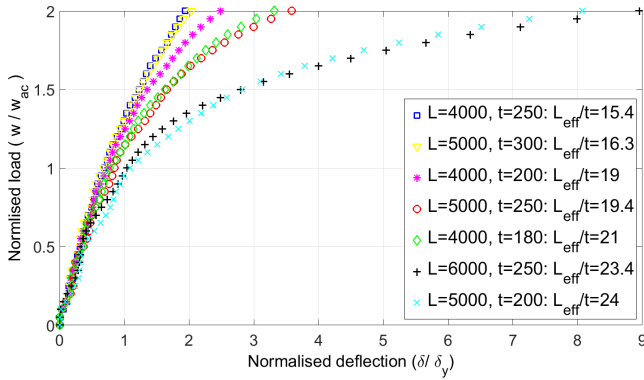


Figure 12. Displacement ductility factor, μ_δ , after corner column removal

349 observed, as displacements are usually less than δ_y . The coefficient of determination of
 350 a linear fit, R^2 , values in Table 5 indicate that there has only been a minor reduction in
 351 the stiffness of the section due to the concrete cracking ($R^2 > 0.958$). As the load is
 352 increased further, displacements in the lower span to depth ratios remain small, while
 353 beyond a L_{eff}/t of 19.4 larger relative displacements, and associated damage occur.

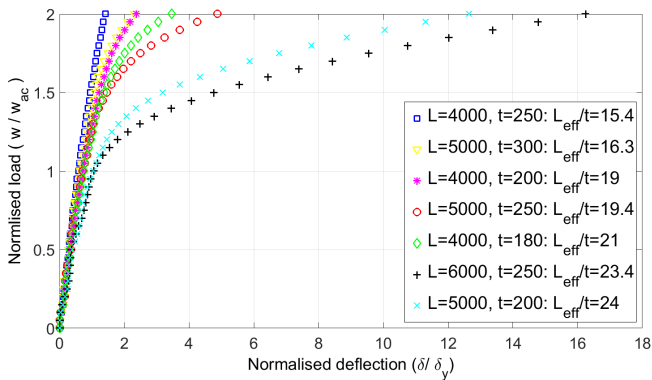
354 For all cases, the nonlinearity in the displacement response starts when the increased
 355 bending moments generate cracking around the adjacent supports. There is then a gradual
 356 reduction in the stiffness as these cracks spread, as shown previously. During this phase,
 357 the underside of the concrete starts to crack, which further reduces the stiffness of the
 358 slab leading to larger deflections. This behaviour was more evident in flexible slabs with
 359 higher span to depth ratios.

360 As geometric nonlinearity, primarily due to the formation of a tensile membrane,
 361 typically only becomes significant beyond displacements of 0.5 times the slab depth,
 362 these results do not suggest this is a key factor. Additionally, it has been noted that
 363 in order for a tensile membrane to be effective, large rotations are required at the
 364 supports which may result punching shear failure before the secondary mechanism forms
 365 (Sagaseta et al. 2016).

366 A similar response is observed from an internal column loss, shown in Figure 13.
 367 In general, with a larger L_{eff}/t , greater normalised displacements occur. However, it
 368 can be seen that while $L_{eff}/t=19.4$ and 21.0 start off similar, by a loading of $2w_{ac}$
 369 the theoretically stiffer model experiences higher relative displacements. The 19.4 case
 370 has a thicker section depth, 250mm compared to 180mm, and hence a higher self weight,

Table 5. Summary of static deflections - Corner removal

Span to depth ratio L_{eff}/t	Yield displacement δ_y/t	δ/t at w_{ac}	R^2 up to w_{ac}	δ/t at $2w_{ac}$
15.4	0.013	0.009	0.995	0.026
16.3	0.021	0.015	0.991	0.043
19.0	0.025	0.018	0.989	0.061
19.4	0.030	0.025	0.984	0.106
21.0	0.032	0.025	0.988	0.105
23.4	0.064	0.067	0.958	0.575
24.0	0.048	0.052	0.980	0.385

**Figure 13.** Displacement ductility factor, μ_δ , after internal column removal

371 which becomes more significant once concrete damage starts to occur. Considering all the
 372 configurations demonstrates that up to a loading of w_{ac} the system remains in the elastic
 373 range, however, once cracking starts to occur a significant nonlinearity is observed.

374 Of further interest is the response of other parts of the structure to a column loss.
 375 Figure 14 shows the normalised displacements against loading after the corner column
 376 has been removed for locations away from the removed column. From Figure 14(a) it is
 377 clear that the relative displacements in the bay adjacent to the one containing the removed
 378 column are very small especially for the stiffest structures. Figure 14(b) shows the results
 379 of locations further from the damaged area. As expected, all the models show a linear
 380 relationship up to w_{ac} . Beyond this point, load is only applied to the bay around the lost
 381 column, and therefore the adjacent bay and the middle bays show a slight uplift, while
 382 the furthest bay on the other side of the structure appears to be unaffected. Of final note is

Table 6. Load factor at first punching shear failure

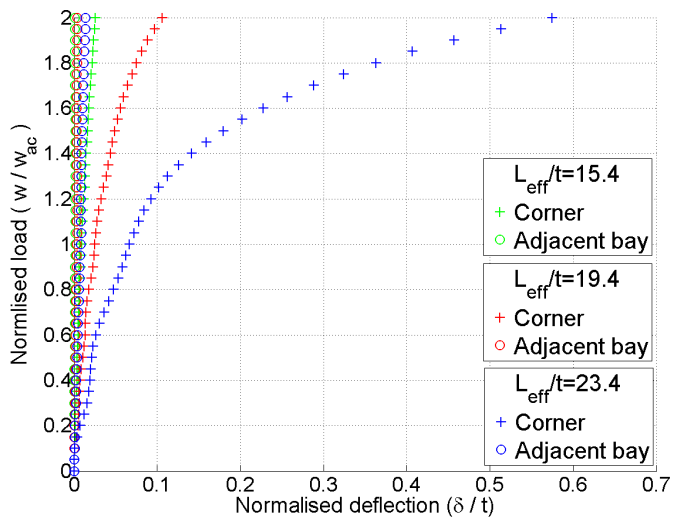
Span (mm)	Thickness (mm)	Removal Location			
		Corner	Internal	Penultimate	Two Column
4000	180	2.0+	2.0+		
	200	2.0+	2.0+		
	250	2.0+	2.0+		
5000	200	2.00	1.95	1.90	1.55
	250	2.0+	2.0+	2.0+	1.80
	300	2.0+	2.0+		
6000	250	1.70	1.55		

383 the response of the adjacent bay for the model with $L_{eff}/t=21.0$. At the highest loading
 384 level the pattern changes from an uplift to a slight downward trend. This is related to the
 385 damage sustained spreading into the adjacent bay and reducing its stiffness. Under other
 386 scenarios the same pattern was seen.

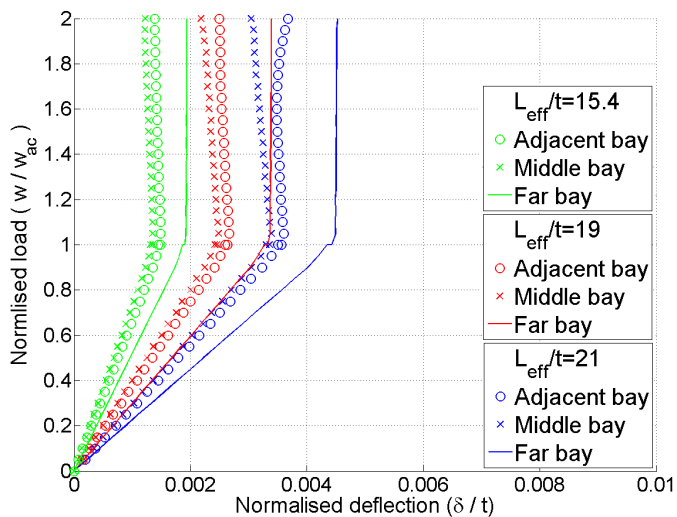
387 *Punching shear assessment*

388 For each scenario the connection rotations were calculated to obtain an estimate for the
 389 punching shear capacity at the remaining columns, according to Equation 5. Figures 15(a)
 390 and 15(b) give examples of the CSCT estimations for connection capacity. As can be seen
 391 for the $L_{eff}/t=24.0$ case, punching shear is predicted at the maximum level of rotation
 392 caused by the full DAF loading of 2.0, while with the longer span case, $L_{eff}/t=23.4$,
 393 punching shear occurs much earlier. Most other cases did not predict failure within the
 394 loading considered. Note that a lower concrete strength would naturally lead to an earlier
 395 punching shear failure.

396 The loading levels at which the first punching shear occurs after a corner or internal
 397 column removal is given in Table 6. It should be noted that if one connection fails,
 398 then failures at other columns are likely to occur leading to a progressive collapse. The
 399 majority of cases were loaded to the full DAF value of 2.0 without any failure occurring
 400 (therefore the failure load is designated as 2.0+, i.e. above the usual DAF), although the
 401 6m span case was noticeably more susceptible. However, the other removal cases show
 402 that internal or penultimate column removals can result in shear failures at lower levels
 403 of loading.

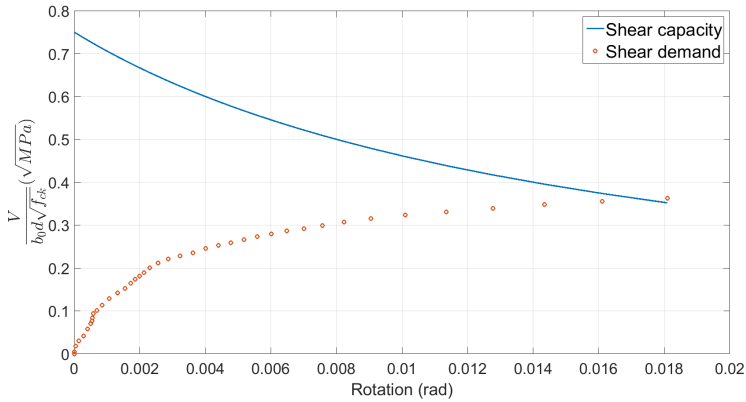


(a) Corner location and adjacent bay

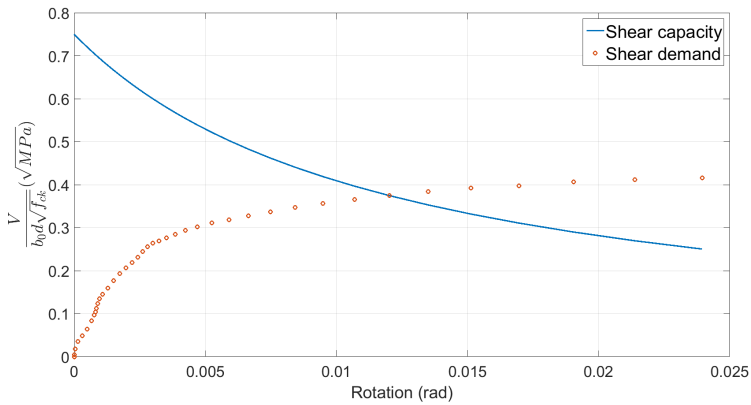


(b) Adjacent, middle and far bays

Figure 14. Normalised displacement at different locations against static loading. Corner column removed with different span to depth ratios



(a) $L=5\text{m}$, $t=200$, $L_{eff}/t=24.0$



(b) $L=6\text{m}$, $t=250$, $L_{eff}/t=23.4y$

Figure 15. CSCT prediction of punching shear demand and capacity after a corner column removal.

404 *Most critical removal locations*

405 By comparing the maximum displacement for each removal condition, an indication
 406 into which situation is most critical can be determined. With $L_{eff}/t=19.4$ all the single
 407 column loss scenarios show a very similar response, as shown in Figure 16. At a loading
 408 of w_{ac} , the corner column loss shows the largest deformation by a small amount, however
 409 all three cases have very similar yield displacements, and remain within the elastic range.

Table 7. Displacement ductility, μ_δ , at different loadings for all column removal locations

Span to depth ratio, L_{eff}/t	Column location	$w = w_{ac}$	$w = 1.5w_{ac}$	$w = 2w_{ac}$
15.4	Corner	0.70	1.23	1.94
	Internal	0.58	0.94	1.41
19.4	Corner	0.86	1.65	3.59
	Internal	0.71	1.46	4.87
	Penultimate	0.75	1.52	4.11
	Two Columns	1.57	4.86	15.37
24.0	Corner	1.08	2.82	8.07
	Internal	1.02	3.18	12.64
	Penultimate	1.08	3.01	10.99
	Two Columns	1.50	5.59	16.68

410 By $2w_{ac}$ the loss of an internal column leads to the highest deflections compared to other
 411 removal cases, except for the stiffest case. Although these differences on the whole are
 412 not very large. Considering the case with $L_{eff}/t=24$, Figure 16 shows that the three cases
 413 have a very similar response at low loading levels, although by w_{ac} they have reached
 414 the yield displacement. Similar to the previous case, an internal column loss is the most
 415 critical scenario which becomes apparent after $1.5w_{ac}$.

416 For further comparison these values are also presented in Table 7. This highlights that
 417 for a single column loss, the displacement ductility demand increases by increasing the
 418 span to depth ratio, up to the accidental load case, w_{ac} , and all slab elements remain close
 419 to the elastic range. By a 50% increase in loading on the damaged bay, the displacements
 420 at the removal locations can increase up to 3 times the yield displacement. With a DAF of
 421 two, currently recommended for static analyses, the displacements exceeded 10 times the
 422 yield displacement, indicating a very strong nonlinear behaviour. The maximum ductility
 423 demands indicate that an internal column removal would be the most critical case for
 424 slabs with L_{eff}/t of 19.4 and 24, which is consistent with the displacement results
 425 presented before. However, corner column loss could lead to higher ductility demands
 426 in the slab elements with lower span to depth ratios (i.e. $L_{eff}/t=15$).

427 The loss of two columns, a corner and a penultimate edge, naturally creates a worse
 428 scenario with deflections higher than any of the other cases, and peak deflections more
 429 than four times the next largest value. This indicates that a structure that is considered
 430 safe against a single column loss could be vulnerable to progressive failures should a
 431 second column fail and if the structure does not have enough ductility to maintain its
 432 integrity.

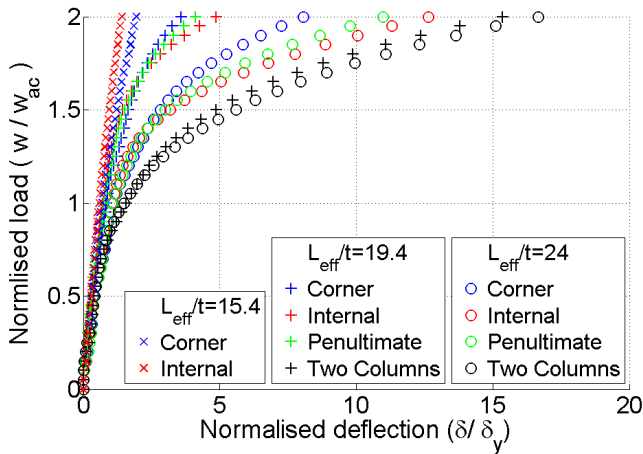


Figure 16. Normalised displacement against loading for different column loss scenarios

433 *Effects of concrete strength*

434 To investigate the effects of concrete strength on the behaviour of flat slabs after a
 435 column loss, a final comparison is made between three different compressive concrete
 436 strengths, based on displacement against loading curves, plotted in Figure 17. Two
 437 removal scenarios are presented for a model with $L_{eff}/t=19.4$. It is shown that up
 438 to w_{ac} there is very little difference in the response of the structures with different
 439 concrete strengths with displacements below, or close to, the yield displacement. Total
 440 variation between cases is less than 3mm for a slab with a depth of 250mm. However,
 441 as the loading is increased further, the lower strength concrete structure shows higher
 442 normalised displacements. Note that the lower concrete strength case had additional
 443 reinforcement to meet design requirements.

444 Of further note is the change in critical column loss scenario between corner and
 445 internal column removal cases. At all concrete strengths the corner loss causes a higher
 446 displacement at low loading levels. However, damage starts to occur at a lower load for
 447 the internal case which reduces its stiffness and causes higher final deflections. As the
 448 changeover point is dependent on the flexural damage to the slab elements, a higher
 449 concrete strength delays this effect.

450 A static analysis provides information on many of the important aspects for progressive
 451 collapse, and is commonly used for design. However, in reality, sudden column loss is a

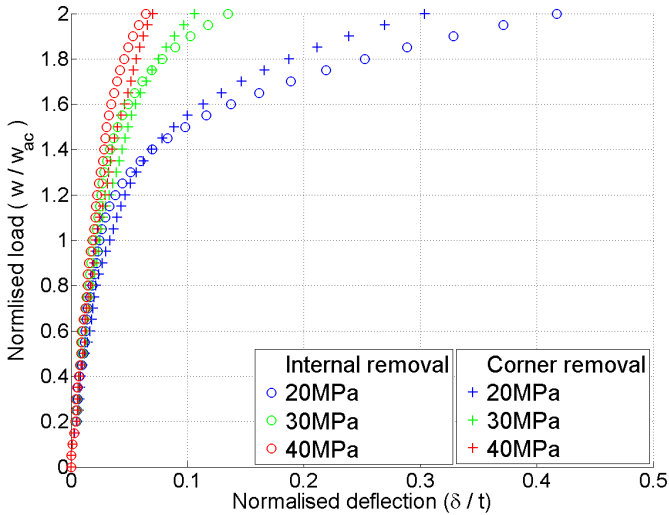


Figure 17. Normalised displacement against static loading for concrete strengths. Corner and internal column removal. $L_{eff}/t=19.4$

452 dynamic event that affects the demand placed on the structure due to inertial effects, and
 453 potentially increases the material strength if high strain rates are involved. The influence
 454 of the dynamic effects on flat slab structure will be addressed in a further paper.

455 Summary and conclusions

456 This study aimed to investigate the nonlinear behaviour of RC flat slab structures after
 457 a sudden column loss event. Non-linear finite element models were developed and
 458 validated against experimental results. It was shown that the models can accurately
 459 simulate the force-displacement response of the flat slabs and predict the location of
 460 concrete cracks and changes in the reaction forces after a column loss event. The
 461 validated FE models were then extended to investigate the effects of different design
 462 parameters such as span length, slab thickness and concrete compressive strength on the
 463 nonlinear response of flat slab structures considering different column loss scenarios.
 464 Based on the results presented in this paper, the following conclusions can be drawn:

- 465 • In general the flat slab systems showed to be robust and could redistribute the
 466 loads after a column loss by utilising alternative load paths. Changing the span to

467 depth ratio did not affect the stress distribution and progression of damage patterns
468 after a column loss. However, by increasing the span to depth ratio the nonlinear
469 behaviour due to cracking occurred earlier.

- 470 • Beyond the elastic limits, damage and a permanent reduction in its stiffness
471 occurred due to cracking of the concrete, with the most critical aspect being the
472 extension of hogging bending stresses to areas that may not have been designed for
473 such conditions. Compared to the corner column loss, an internal column removal
474 affected a larger area of the slab and therefore led to higher displacement demands.
475 Increasing the span to depth ratio (i.e. more flexible slabs) caused an increase in the
476 displacement ductility demand after both corner and internal column. In general,
477 the relative displacements in the bays adjacent to the one containing the removed
478 column are very small especially for the stiff slabs with low span to depth ratios.
- 479 • There was no significant difference in the reaction force demands for structures
480 with different span to depth ratios. After a corner or an internal column loss, the
481 orthogonally adjacent columns to the removed location experienced the largest
482 increase in their vertical loading (by up to 3 times after accounting for dynamic
483 effects). It was shown that removing two columns simultaneously may not be the
484 most critical design scenario as the vertical loads can be redistributed to more
485 columns and reduce the demand on a single location.
- 486 • For long span slabs (over 5 m), the punching shear may occur at DAF values lower
487 than the 2.0 suggested by the design guidelines. However, in shorter span slabs
488 the punching shear was not usually a dominant failure mode. It was shown that, in
489 general, the internal or penultimate column removals can result in shear failures at
490 lower levels of loading.
- 491 • The results suggest that the most critical removal location depends on the slab
492 geometry with an internal column removal case causing the largest nonlinear
493 behaviour for stiffer slabs, and a corner column removal for more flexible
494 slabs. Additionally, the use of low strength concrete results in structures more
495 prone to progressive collapse, even after accounting for an increase in flexural
496 reinforcement.

497 **Acknowledgements**

498 The authors would like to acknowledge the Early Career Research and Knowledge
499 Transfer grant awarded by the University of Nottingham to Dr. Hajirasouliha that funded

500 the project. They are also are grateful for access to the University of Nottingham High
501 Performance Computing Facility, on which the simulations were run.

502 References

- 503 Eurocode 1992. BS EN 1992: Eurocode 2 - Design of concrete structures - Part 1-1: General rules
504 and rules for buildings, 2004.
- 505 U. Cicekli, G. Z. Voyiadjis, and R. K. A. Al-Rub. A plasticity and anisotropic damage model for
506 plain concrete. *International Journal of plasticity*, 23(10):1874–1900, 2007.
- 507 P. X. Dat and T. K. Hai. Membrane actions of RC slabs in mitigating progressive collapse of
508 building structures. *Engineering Structures*, 55:107–115, 2013.
- 509 Fédération Internationale du Béton. *Model code 2010 : final draft*. Bulletin / Federation
510 Internationale du Beton ; 65-66. International Federation for Structural Concrete (fib), 2012.
511 Prepared by fib Special Activity Group 5, New Model Code.
- 512 D. M. V. Faria, V. J. G. Lucio, and A. P. Ramos. Post-punching behaviour of flat slabs strengthened
513 with a new technique using post-tensioning. *Engineering Structures*, 40:383–397, 2012.
- 514 G. Flint, A. Usmani, S. Lamont, B. Lane, and J. Torero. Structural response of tall buildings to
515 multiple floor fires. *Journal of Structural Engineering-ASCE*, 133(12):1719–1732, 2007.
- 516 Feng Fu. 3-d nonlinear dynamic progressive collapse analysis of multi-storey steel composite
517 frame buildingsparametric study. *Engineering Structures*, 32(12):3974–3980, 2010.
- 518 N. J. Gardner, J. Huh, and L. Chung. Lessons from the Sampoong department store collapse.
519 *Cement & Concrete Composites*, 24(6):523–529, 2002.
- 520 Aikaterini S Genikomsou and Maria Anna Polak. Finite element analysis of punching shear of
521 concrete slabs using damaged plasticity model in abaqus. *Engineering Structures*, 98:38–48,
522 2015.
- 523 N. M. Hawkins and D. Mitchell. Progressive Collapse of Flat-Plate Structures. *Journal of the*
524 *American Concrete Institute*, 76(7):775–808, 1979.
- 525 T. Jankowiak and T. Lodygowski. Identification of parameters of concrete damage pasticity
526 constitutive model. *Foundations of Civil and Enviromental Engineering*, (6):53–69, 2005.
- 527 L. Keyvani, M. Sasani, and Y. Mirzaei. Compressive membrane action in progressive collapse
528 resistance of RC flat plates. *Engineering Structures*, 59:554–564, 2014.
- 529 S. Kokot, A. Anthoine, P. Negro, and G. Solomos. Static and dynamic analysis of a reinforced
530 concrete flat slab frame building for progressive collapse. *Engineering Structures*, 40:205–
531 217, 2012.

- 532 Leslaw Kwasniewski. Nonlinear dynamic simulations of progressive collapse for a multistory
533 building. *Engineering Structures*, 32(5):1223–1235, 2010.
- 534 J. H. Lee and G. L. Fenves. Plastic-damage model for cyclic loading of concrete structures. *Journal*
535 *of Engineering Mechanics-ASCE*, 124(8):892–900, 1998.
- 536 J. Li and H. Hao. Numerical study of structural progressive collapse using substructure technique.
537 *Engineering Structures*, 52:101–113, 2013.
- 538 J. Liu, Y. Tian, and S. L. Orton. Resistance of flat-plate buildings against progressive collapse. ii:
539 system response. *Journal of Structural Engineering*, 141(12):04015054, 2015.
- 540 J. Lubliner, J. Oliver, S. Oller, and E. Onate. A Plastic-Damage Model for Concrete. *International*
541 *Journal of Solids and Structures*, 25(3):299–326, 1989.
- 542 N. F. S. Mamede, A. P. Ramos, and D. M. V. Faria. Experimental and parametric 3D nonlinear
543 finite element analysis on punching of flat slabs with orthogonal reinforcement. *Engineering*
544 *Structures*, 48:442–457, 2013.
- 545 K Micallef, J Sagaseta, M Fernández Ruiz, and A Muttoni. Assessing punching shear failure in
546 reinforced concrete flat slabs subjected to localised impact loading. *International Journal of*
547 *Impact Engineering*, 71:17–33, 2014.
- 548 Y. Mirzaei and M. Sasani. Progressive collapse resistance of flat slabs: modeling post-punching
549 behavior. *Computers and Concrete*, 12(3):351–375, 2013.
- 550 D. Mitchell and W. D. Cook. Preventing Progressive Collapse of Slab Structures. *Journal of*
551 *Structural Engineering-ASCE*, 110(7):1513–1532, 1984.
- 552 A. Muttoni. Punching shear strength of reinforced concrete slabs without transverse reinforcement.
553 *ACI Structural Journal*, 105(4):440–450, 2008.
- 554 H. Okamura and K. Maekawa. Nonlinear-Analysis and Constitutive Models of Reinforced-
555 Concrete. *Computer Aided Analysis and Design of Concrete Structures, Vols 1 and 2*, pages
556 831–850, 1990.
- 557 P Olmati, J Sagaseta, D Cormie, and AEK Jones. Simplified reliability analysis of punching in
558 reinforced concrete flat slab buildings under accidental actions. *Engineering Structures*, 130:
559 83–98, 2017.
- 560 T. W. Park. Inspection of collapse cause of Sampoong Department Store. *Forensic Science*
561 *International*, 217(1-3):119–126, 2012.
- 562 A. T. Pham and K. H. Tan. Experimental study on dynamic responses of reinforced concrete frames
563 under sudden column removal applying concentrated loading. *Engineering Structures*, 139:31
564 – 45, 2017.

- 565 K. Qian and B. Li. Slab Effects on Response of Reinforced Concrete Substructures after Loss of
566 Corner Column. *ACI Structural Journal*, 109(6):845–855, 2012.
- 567 K. Qian and B. Li. Performance of Three-Dimensional Reinforced Concrete Beam-Column
568 Substructures under Loss of a Corner Column Scenario. *Journal of Structural Engineering-
569 ASCE*, 139(4):584–594, 2013.
- 570 M. F. Ruiz, Y. Mirzaei, and A. Muttoni. Post-Punching Behavior of Flat Slabs. *ACI Structural
571 Journal*, 110(5):801–811, 2013.
- 572 J Russell. *Progressive collapse of reinforced concrete flat slab structures*. PhD thesis, University
573 of Nottingham, 2015.
- 574 JM Russell, JS Owen, and I Hajirasouliha. Experimental investigation on the dynamic response of
575 rc flat slabs after a sudden column loss. *Engineering Structures*, 99:28–41, 2015.
- 576 J. Sagaseta, N Ulaeto, and J Russell. Structural robustness of concrete flat slab structures. In
577 *International Symposium on Punching Shear of Structural Concrete Slabs - Honoring Neil
578 Hawkins (In fib bulletin 81)*, pages 273–298, 2016.
- 579 M. Sasani, M. Bazan, and S. Sagiroglu. Experimental and analytical progressive collapse
580 evaluation of actual reinforced concrete structure. *ACI Structural Journal*, 104(6):731–739,
581 2007.
- 582 Simulia. ABAQUS Inc. User Manuel, version 6.10, 2010.
- 583 Y. P. Su, Y. Tian, and X. S. Song. Progressive Collapse Resistance of Axially-Restrained Frame
584 Beams. *ACI Structural Journal*, 106(5):600–607, 2009.
- 585 N. Trivedi and R. K. Singh. Prediction of impact induced failure modes in reinforced concrete slabs
586 through nonlinear transient dynamic finite element simulation. *Annals of Nuclear Energy*, 56:
587 109–121, 2013.
- 588 M. Tsai and B. Lin. Dynamic amplification factor for progressive collapse resistance analysis of
589 an rc building. *The Structural Design of Tall and Special Buildings*, 18(5):539–557, 2009.
- 590 US General Services Administration (GSA). Alternate path analysis & design guidelines for
591 progressive collapse resistance, 2013.
- 592 H. R. Valipour and S. J. Foster. Finite element modelling of reinforced concrete framed structures
593 including catenary action. *Computers & structures*, 88(9):529–538, 2010.
- 594 R. Whittle. *Failures in concrete structures : case studies in reinforced and prestressed concrete*.
595 CRC Press, 2013. Includes bibliographical references and index.
- 596 W. J. Yi, Q. F. He, Y. Xiao, and S. K. Kunnath. Experimental study on progressive collapse-
597 resistant behavior of reinforced concrete frame structures. *ACI Structural Journal*, 105(4):
598 433–439, 2008.